RSC Advances

ROYAL SOCIETY OF CHEMISTRY

www.rsc.org/advances

Journal Name

RSCPublishing

ARTICLE

Mesoporous $Ni_{0.3}Co_{2.7}O_4$ hierarchical structures for effective nonenzymatic glucose detection

Cite this: DOI: 10.1039/x0xx00000x

Yuanying Liu, [a] Youjuan Zhang, [a] Ting Wang, [a] Panpan Qin, [a] Qifei Guo [a] and Huan Pang* [a, b]

Received 00th January 2012,
Accepted 00th January 2012

DOI: 10.1039/x0xx00000x

www.rsc.org/

Mesoporous nickel cobalt oxide hierarchical structures are successfully synthesized by a controlled calcination of nickel cobalt oxalate hydrate hierarchical structures. More importantly, mesoporous nickel cobalt oxide hierarchical structures modified electrode shows remarkable electrochemical performance for nonenzymatic glucose detection. The electrode modified with mesoporous $Ni_{0.3}Co_{2.7}O_4$ hierarchical structures shows a low detection limit of 1.0 μM glucose, good sensitivity of 206.5 $mA \cdot mM^{-1} \cdot cm^{-2}$, and good selectivity.

Introduction

Recently, glucose detection is essential in biotechnology, the food field and clinical diagnostics.[1] Great interest has been devoted to glucose sensors, since the enzyme electrode was reported for measuring glucose.[2-4] The amperometric glucose sensor is one of the most promising techniques among various glucose testing methodologies, in which the enzyme glucose oxidase (GOD) is used as the crucial constituent to catalyze the oxidation of glucose to gluconolactone.[5, 6] However, the activity of the enzyme GOD can be easily affected by temperature, humidity, and pH value due to the intrinsic features of enzymes.[7, 8] Therefore, a nonenzymatic glucose sensor, especially for a long-term stable glucose sensor, should be emphasized in future research. Nanomaterials, which have conspicuous physical and chemical properties compared to their bulk counterparts, have been applied to sensors for glucose detection. Such as, Au nanoparticles, Cu micropuzzles, CuS nanotubes carbon nanotubes and nitrogen-doped carbon–copper nanohybrids have been used to modify electrodes as nonenzymatic sensors and demonstrated to be very effective for glucose detection, which suggests that nanomaterials might provide potential candidates for application as nonenzymatic glucose sensors.[9-16]

Mixed transition metal oxides (MTMOs), typically ternary metal oxides with two different metal cations, have received an upsurge of interest in recent years due to their promising roles in many electrochemical applications, such as lithium-ion batteries, supercapacitors, metal–air batteries, fuel cells and sensors.[17–24] Usually, MTMOs materials exhibit a formula of $A_xB_{3-x}O_4$ in a spinel structure, in which A and B represent two different transition metals such as Fe, Ni, Co, Mn, Zn, etc. The coupling of two metal species could render the MTMOs with rich redox reactions and improved electronic conductivity, which are beneficial to electrochemical applications. More importantly, the various combinations of the cations and the tunable stoichiometric/non-stoichiometric compositions in the MTMOs provide vast opportunities to manipulate the physical/chemical properties. The ternary nickel cobaltite $NiCo_2O_4$, as a typical kind of MTMOs materials, has been intensively investigated as a high performance electrochemical energy material. [21, 25–35] When compared with binary metal oxides NiO and Co_3O_4, ternary $NiCo_2O_4$ exhibits higher electrical conductivity and improved electrochemical activity, which originates from the co-existence of the Ni and Co species.[21, 36] In addition, the spinel nickel cobalt oxide can be considered as Co_3O_4 with Co partially substituted by Ni. Therefore, mixed nickel cobalt oxides with compositions other than $NiCo_2O_4$ are also anticipated with great potential for electrochemical sensors, but there are nearly on reports on this.

Herein, we report the facile synthesis of mesoporous nickel cobalt oxide ($Ni_{0.3}Co_{2.7}O_4$) hierarchical structures with remarkable electrochemical performance for nonenzymatic

glucose detection. Nickel cobalt oxalate hydrate ($Ni_{0.1}Co_{0.9}C_2O_4{\cdot}nH_2O$) is successfully synthesized as the precursor, followed by a controlled calcination process to transform to mesoporous nickel cobalt oxide hierarchical structures. The electrode modified with mesoporous $Ni_{0.3}Co_{2.7}O_4$ hierarchical structures is especially effective for glucose sensing, as it shows a low detection limit of 1.0 μM, good sensitivity of 206.5 $mA{\cdot}mM^{-1}{\cdot}cm^{-2}$, and good selectivity.

Experimental

Materials synthesis

Synthesis of $Ni_{0.1}Co_{0.9}C_2O_4{\cdot}nH_2O$ hierarchical structures: Firstly, 1 mL of 0.1 M $Ni(NO_3)_2$ aqueous solution, 9 mL of 0.1 M $CoCl_2$ aqueous solution and 10 mL of ethanol (EtOH) were mixed for 30 min at room temperature. After that, 10 mL of 0.1 M $Na_2C_2O_4$ solution was quickly poured into the above solution. A pink precipitate (Denoted by P) was collected after reaction for 1 h, and used as the precursor to synthesize mixed nickel cobalt oxide hierarchical structures.

Synthesis of mesoporous nickel cobalt oxide hierarchical structures: The $Ni_{0.1}Co_{0.9}C_2O_4{\cdot}nH_2O$ precursor was heated from room temperature to 400 °C with a heating rate of 1 °C min^{-1} and maintained at 400 °C for 10 min, and the obtained product is denoted as M.

Electrochemical sensor electrode preparation

Bare carbon paste electrode (B-CPE), 1.8 mm diameter, was prepared using graphite powder, liquid paraffin, with a ratio of 75:25 (w/w); mesoporous $Ni_{0.3}Co_{2.7}O_4$ hierarchical structures - carbon paste electrode (M-CPE), 1.8 mm diameter, was prepared using graphite powder, liquid paraffin, and mesoporous $Ni_{0.3}Co_{2.7}O_4$ hierarchical structures with a ratio of 74:25:1 (w/w). The electrochemical cell was assembled with a conventional three-electrode system: a Ag/AgCl/KCl (saturated) reference electrode and a platinum coil as an auxiliary electrode. 0.1 M NaOH was used for determination of glucose.

Material characterizations

The morphology of as-prepared samples was observed using a JEOL JSM-6701F field-emission scanning electron microscope (FESEM) at an acceleration voltage of 5 kV. The elemental analysis was carried out using a Bruker-QUANTAX, energy dispersive X-ray spectroscope (EDS) attached to a FESEM. The phase analysis of the samples was performed by X-ray diffraction (XRD) on a Rigaku-Ultima III with Cu Ka radiation (λ=1.5418 Å). Transmission electron microscopy (TEM) and high resolution TEM (HRTEM) images were captured on a JEOL JEM-2100 microscope at an acceleration voltage of 200 kV. Nitrogen adsorption–desorption measurements were performed on a Gemini VII 2390 Analyzer at 77 K. Thermogravimetric analysis (TGA) was carried out in air up to 800 °C using a NETZSCH STA 409 PC instrument with a heating rate of 5 °C·min^{-1}. Inductively coupled plasma atomic emission spectroscopy (ICP-AES) analysis was carried out on a PerkinElmer Optima 8000.

Results and discussion

The whole synthesis process of hierarchical architecture precursor was under room temperature without using any templates or surfactants (seen experiment section). The powder X-ray diffraction pattern of as-prepared precursor is shown in **Figure S1**, and all peaks are good in agreement with the corresponding standard cards, JCPDS 01-0296 & 01-0299 for $CoC_2O_4{\cdot}2H_2O$ & $NiC_2O_4{\cdot}2H_2O$. The morphology of $Co_{0.9}Ni_{0.1}C_2O_4{\cdot}nH_2O$ was observed by SEM images in **Figure 1**. The hierarchical architecture precursor assembled by many nanorods has been successfully synthesized in Figure 1. These nanorods have assembled together and formed many nanogaps in Figure 1b. And the size of a single microflower is 3~4 μm in Figure 1b.

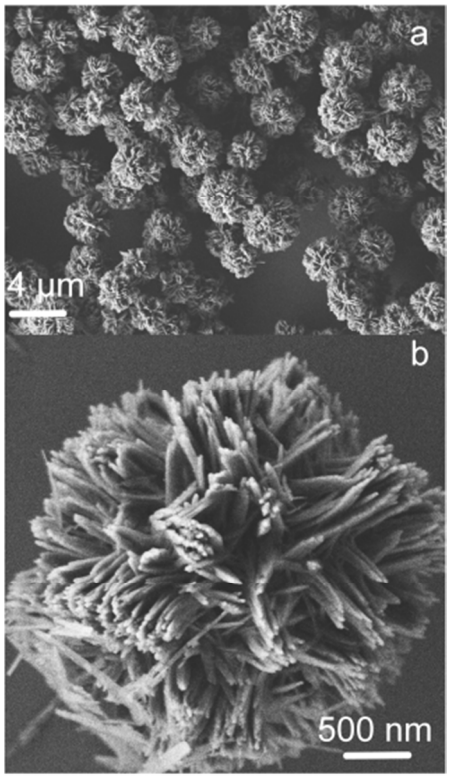

Figure 1 SEM images of as-prepared precursors

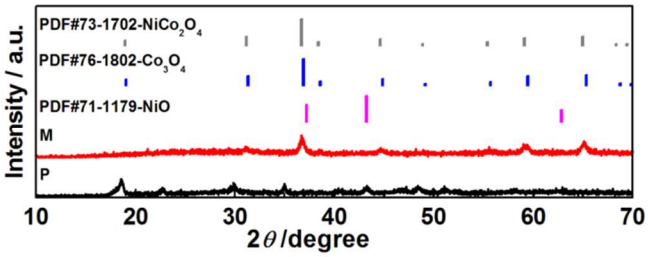

Figure 2 XRD patterns of as-prepared the precursor (Denoted by **P**), the product obtained after the calcination under 400 °C (Denoted by **M**), and standard patterns of NiO, Co_3O_4, and $NiCo_2O_4$.

Mesoporous nickel cobalt oxide hierarchical architectures (Denoted by **M**) are obtained by the calcination of air the oxalate precursors at 400 °C, and their XRD patterns are shown in **Figure 2**. The XRD patterns of the sample as given in **Figure 2** are similar to the standard patterns of $NiCo_2O_4$ and Co_3O_4, indicating that the mixed nickel cobalt oxide also adopts the spinel structure with similar lattice constants. Quantitative analysis by EDS confirms the Co/Ni atomic ratio of about 9 for all the three nickel cobalt oxide samples. The Co/Ni atomic ratio is further analyzed and confirmed by ICP-AES, which is according with EDS results.

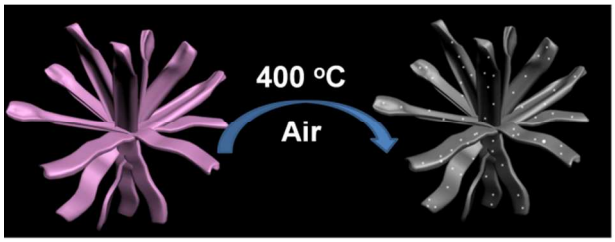

Scheme 1 A simple synthesis skeleton of M.

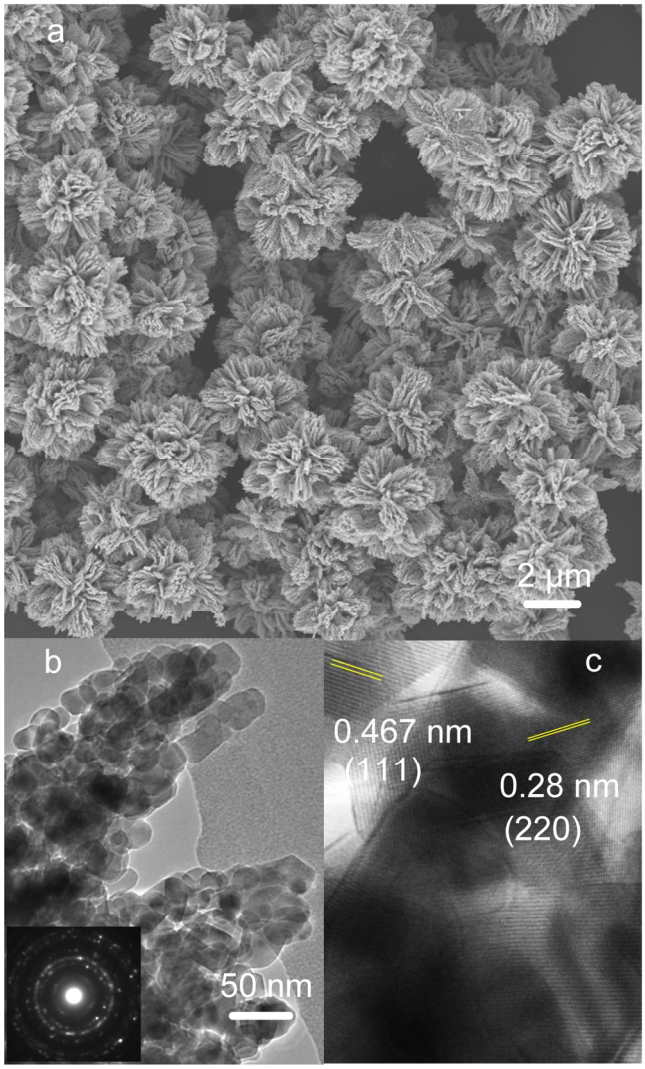

Figure 3 a) A SEM image of M, b) A TEM image of M, in inset of b-corresponding selected area diffraction (SAED) patterns, and c) The corresponding HRTEM image.

Scheme 1 shows a simple skeleton of the whole synthesis of mesoporous nickel cobalt oxide hierarchical architectures from $Co_{0.9}Ni_{0.1}C_2O_4{\cdot}nH_2O$ hierarchical architecture precursor with the thermal condition. There might be some porous structures generated after gas released. And to more clearly and correctly describe porous properties of as-prepared materials, SEM and TEM images of all samples are shown in **Figure 3**. In Figure 3a, the morphology of hierarchical architecture was maintained after the calcination in the air, but the surface of M has changed and becomes coarse. M also has a hierarchical architecture with 3~4 μm in Figure 3a. From TEM images of Figure 3b, pores of M are distributed homogeneously among the small primary particles (several nanometers) throughout the whole hierarchical architecture (several micrometers). There are thousands of pores in a hierarchical architecture for M. The selected area diffraction (SAED) patterns of M are shown in inset of Figure 3b. It is clear that M has the good crystalline, and the corresponding interplanar spacing image of M also improved its good crystalline.

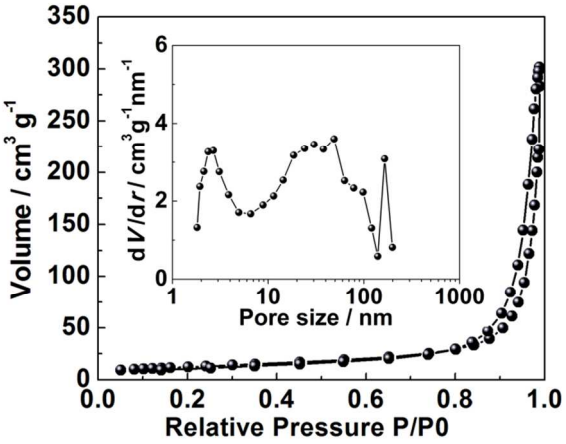

Figure 4 N_2 adsorption–desorption isotherms of as-prepared M and the corresponding Barrett–Joyner–Halenda (BJH) pore size distribution curve (inset).

To gain further insight into the porous structure and pore size distribution of M, Brunauer–Emmett–Teller (BET) measurements were performed to examine its specific structural properties. The products show a distinct hysteresis in the larger range ca. 0.8–1.0 P/P_0 in inset of **Figure 4**, indicating the presence of mesopores possibly formed by porous stacking of component nanoparticles. The BET surface area of M is 43.7 $m^2{\cdot}g^{-1}$, and it makes an efficient contact of activated materials with electrolyte. The corresponding Barrett–Joyner–Halenda (BJH) pore size distribution curve is shown in inset of Figure 4. M mainly has the range of mesopores (3–10 nm and 18-50 nm). It is well known that the pore structure has great effect on the electrochemical performance of the carbon materials. Pores with different sizes play different roles in the electrochemical process.[37-40]

Figure S3 exhibits the electrochemical impedance spectroscopy (EIS) of the the mesoporous mesoporous $Ni_{0.3}Co_{2.7}O_4$ hierarchical structures modified carbon paste electrode (M-CPE) and the bare carbon paste electrode (CPE). As shown in **Figure S3**, after the modification, the semicircle diameter of EIS shows an increase compared with the bare CPE electrode. The impedance changes of the modification process show that the mesoporous mesoporous $Ni_{0.3}Co_{2.7}O_4$ hierarchical structures attach to the electrode surface according to the in the same way as in previous literature. As shown in a curve of **Figure 5**a, on the M-CPE, there appears a strong peak for the glucose in 0.1 M NaOH solution. The M-CPE curve, the oxidation peak potential of glucose on mesoporous $Ni_{0.3}Co_{2.7}O_4$ hierarchical structures modified electrode is at 0.60 V in Figure 5a, while that of CPE does not show. Fast and sensitive glucose detection capability of the M-CPE was assessed by recording the current–time responses upon the successive addition of various concentrations of glucose (Figure 5b, c). At applied potential of 0.60 V, the oxide currents at the M-CPE increase gradually during the successive additions of glucose into the

stirring NaOH solution, and reach the maximum steady-state current within 3 s. The obtained linear range of Figure 5d spans the concentration of glucose from 1.0 μM to 2.55 mM. What is more, the linear equation is R=0.9972, Current I (μA) = 1.441-8.52C (mM) in Figure 5d, and the calculated sensitivity is 206.5 mA·mM^{-1}·cm^{-2} for M-CPE.

One of the major challenges in nonenzymatic glucose detection is to eliminate the electrochemical response generated by some easily oxidizable endogenous interfering compounds such as vitamin c (Vc), dopamine (DA), uric acid (UA), Glutathione (GSH), Cysteine (Cys) and NaCl. These interfering species can produce the oxidation current comparable to that of glucose, attributing to their higher electron transfer rates. It is expected that M-CPE with a high active surface pots can favor a kinetically controlled sluggish reaction (the oxidation of glucose) to a greater extent than diffusion controlled reactions (the oxidation of interfering species). (***Cautions***: To complete the picture of how these potential interferents behave, we do not include the redox potential for each. Some might be expected to be oxidized at 0.6 V, some will not.) To verify this, we investigated the amperometric responses of the M-CPE at an applied potential of +0.60 V in 0.1 M NaOH solution with continuous additions of 100 μM glucose, 200 μM Vc, 200 μM DA, 200 μM UA, 200 μM GSH, 200 μM Cys, 200 μM NaCl, and 100 μM glucose. Compared with the other six interfering species, a remarkable glucose signal was obtained from the current response in Figure 5e. Compared to glucose, the interfering species yielded current response for M electrode ranging from 0% (Vc), 0.1% (DA), 0.1% (UA), 0.1% GSH, 0.5% (Cys) to 0.2% (NaCl). These results indicated that the M-CPE could be used for the selective and sensitive detection of glucose with negligible interference from Vc, DA, UA, GSH, Cys, and NaCl. However, normal human blood glucose is 3.89-6.1 mmol L^{-1}and NaCl is present at >0.1 M. So, we have added the interferent test (The concentration of NaCl solution is 0.2 M, seen in **Figure S4**). Compared to glucose, the interfering specie (0.2 M NaCl) yields a much weaker current response. The M-CPE owns good catalytic specificity to glucose due to different functional groups between GLU, Vc, DA, UA, GSH and Cys which show different current responses at our electrochemical condition. However, the M-CPE does not show the high selective and sensitive detection of glucose in that the interferring species (fructose, lactose) cause innegligible interferring current on the electrode as seen in **Figure S5**. In Figure 5f, the curve is the stability of the response current for M-CPE after the addition glucose solution (100 μM) during 3600 seconds. It is seen that the specific response current after 600 s is 93.4% of the initial response current, and only 18.8% loss after 3600 seconds, which is stable enough to the application for the electrochemical sensor of glucose.

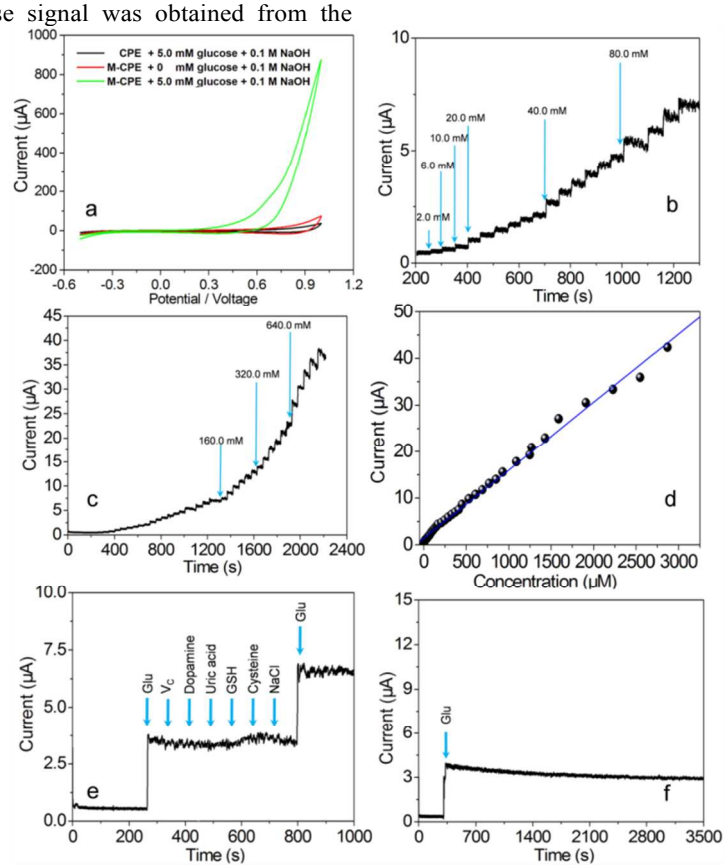

Figure 5 a) Cyclic voltammograms of the M modified carbon paste electrode (M-CPE), carbon paste electrode (CPE) in 0.1 M NaOH solution with (green line, red line) and without (black line) 5.0 mM glucose at a scan rate of 50 mV s^{-1}, b) Current–time response of the M-CPE at potential of 0.60 V on successive injection of different amounts of glucose into stirring 0.1 M NaOH solution from 200 s to 1200 s, c) 0 s to 2300 s, d) A plot of electrocatalytic current of glucose vs its concentrations in the range of 1.0 μM to 2.55 mM, e) Current-time curves for the M-CPE exposed to 100 μM glucose, 200 μM Vc, 200 μM DA, 200 μM UA, 200 μM GSH, 200 μM Cys, 200 μM NaCl, and 100 μM glucose, and f) The stability of the response current for M-CPE after the addition glucose solution (0.1 mM) during 3600 s.

Journal Name

RSCPublishing

ARTICLE

Conclusions

In this work, mesoporous $Ni_{0.3}Co_{2.7}O_4$ architectures are successfully prepared by annealing the nickel cobalt oxalate hydrate composites precursors. As results of specific nanosurface/interface characteristics and conductivity of as-prepared mesoporous $Ni_{0.3}Co_{2.7}O_4$ architectures, mesoporous $Ni_{0.3}Co_{2.7}O_4$ architectures-M can enhance the electron transfer. The measurement of electrochemical sensor of mesoporous $Ni_{0.3}Co_{2.7}O_4$ architectures is an interesting work, which illustrates mesoporous $Ni_{0.3}Co_{2.7}O_4$ architectures can be successfully applied as electroactive materials for nonenzyme glucose sensor. It is a good example to prove that physical and chemical properties of nano/microstructured materials are related to their structures, and the precise control of morphology of nanomaterials will allow for control of the performance. Exploring the electrochemical characteristics of novel nano/micromaterials may direct a new generation of nonenzyme glucose sensor.

Acknowledgements

This work is supported by the Program for New Century Excellent Talents from the Ministry of Education (**NCET**-13-0645) and National Natural Science Foundation of China (**NSFC**-21201010), Program for Innovative Research Team (in Science and Technology) in University of Henan Province (**14IRTSTHN004**), the Science & Technology Foundation of Henan Province (122102210253, 13A150019), the China Postdoctoral Science Foundation (2012M521115), and the Opening Research Foundations of State Key Laboratory of Coordination Chemistry (Nanjing University).

Notes and references

[a] College of Chemistry and Chemical Engineering, Anyang Normal University, Anyang, 455000, Henan, P. R. China.

[b] State Key Laboratory of Coordination Chemistry, Nanjing University, Nanjing, 210093, Jiangsu, P. R. China.

*E-mail: huanpangchem@hotmail.com

† Electronic Supplementary Information (ESI) available: [details of any supplementary information available should be included here]. See DOI: 10.1039/b000000x/

1. Safavi, N. Maleki and E. Farjami, *Biosens. Bioelectron.*, 2009, **24**, 1655.
2. P. Si, Y. J. Huang, T. H. Wang and J. M. Ma, *RSC Advances*, 2013, **3**, 3487
3. Q. Shao, P. Wu, X. Xu, H. Zhang and C. X. Cai, *Phys. Chem. Chem. Phys.*, 2012, **14**, 9076-9085.
4. M. Zhang, A. Smith and W. Gorski, *Anal. Chem.*, 2004, **76**, 5045.
5. D. Lee, J. Lee, J. Kim, J. Kim, H. B. Na, B. Kim, C. H. Shin, J. H. Kwak, A. Dohnalkova, J. W. Grate, T. Hyeon and H. S. Kim, *Adv. Mater.*, 2005, **17**, 2828.
6. H. N. Choi, J. H. Han, J. A. Park, J. M. Lee and W. Y. Lee, *Electroanalysis*, 2007, **19**, 1757.
7. J. X. Wang, X. W. Sun, X. P. Cai, Y. Lei, L. Song and S. S. Xie, *Electrochem. Solid-State Lett.*, 2007, **10**, J58.
8. E. Reitz, W. Jia, M. Gentile, Y. Wang and Y. Lei, *Electroanalysis*, 2008, **20**, 2482.
9. B. K. Jena and C. R. Raj, *Chem.–Eur. J.*, 2006, **12**, 2702.
10. Y. P. Sun, H. Buck and T. E. Mallouk, *Anal. Chem.*, 2001, **73**, 1599.
11. X. J. Zhang, G. F. Wang, A. X. Gu, Y. Wei and B. Fang, *Chem. Commun.*, 2008, 5945.
12. C. K. Tan, K. P. Loh and T. T. L. John, *Analyst*, 2008, **133**, 448.
13. H. Pang, Q. Lu, J. J. Wang, Y. C. Li, F. Gao, *Chem. Commun.*, 2010, **46**, 2010-2012.
14. C. Z. Wei, Y. Y. Liu, X. R. Li, J. H. Zhao, Z. Ren and H. Pang, *ChemElectroChem*, 2014, DOI: 10.1002/celc.201300211.
15. L. Meng, J. Jin, G. X. Yang, T. H. Lu, H. Zhang and C. Cai, *Anal. Chem*., 2009, 81, 7271–7280.
16. Y. J. Hu, J. Jin, P. Wu, H. Zhang, C. X. Cai, *Electrochimica Acta*, 2010, 56, 491-500
17. X. F. Xia, W. Lei, Q. L. Hao, W. J. Wang and X. Wang, *Electrochimica Acta*, 2013, **99**, 253-261.
18. J. H. Jiang, W. D. Shi, S. Y. Song, Q. L. Hao, W. Q. Fan, X. F. Xia, X. Zhang, Q. Wang, C. B. Liu, D. Yan, *J. Power Sources*, 2014, **248**, 1281-1289.
19. L. Zhou, D. Zhao and X. W. Lou, *Adv. Mater.*, 2012, **24**, 745.
20. Y. Liang, H. Wang, J. Zhou, Y. Li, J. Wang, T. Regier and H. Dai, *J. Am. Chem. Soc.*, 2012, **134**, 3517.
21. T.-Y. Wei, C.-H. Chen, H.-C. Chien, S.-Y. Lu and C.-C. Hu, *Adv. Mater.*, 2010, **22**, 347.
22. Y. T. Zhang, L. Q. Luo, Z. Zhang, Y. P. Ding, S. Liu, D. M. Deng, H. B. Zhao and Y. G. Chen, *J. Mater. Chem. B*, 2014, **2**, 529-53
23. Q. F. Li, L. X. Zeng, J. C. Wang, D. P. Tang, B. Q. Liu, G. N. Chen and M. D. Wei, *ACS Appl. Mater. Interfaces*, 2011, **3**, 1366–1373
24. L. J. Chen, B. Sun, X. D. Wang, F. M. Qiao and S. Y. Ai, *J. Mater. Chem. B*, 2013, **1**, 2268-2274
25. H.-C. Chien, W.-Y. Cheng, Y.-H. Wang and S.-Y. Lu, *Adv. Funct. Mater.*, 2012, **22**, 5038.
26. C. Wang, X. Zhang, D. Zhang, C. Yao and Y. Ma, *Electrochim.Acta*, 2012, **63**, 220.
27. H.-W. Wang, Z.-A. Hu, Y.-Q. Chang, Y.-L. Chen, H.-Y. Wu, Z.-Y. Zhang and Y.-Y. Yang, *J. Mater. Chem.*, 2011, **21**, 10504.
28. X. Wang, X. Han, M. Lim, N. Singh, C. L. Gan, M. Jan and P. S. Lee, *J. Phys. Chem. C*, 2012, **116**, 12448.
29. G. Zhang and X. W. Lou, *Adv. Mater.*, 2013, **25**, 976.
30. Q. Lu, Y. Chen, W. Li, J. G. Chen, J. Q. Xiao and F. Jiao, *J. Mater. Chem. A*, 2013, **1**, 2331.
31. Y. Q. Wu, X. Y. Chen, P. T. Ji and Q. Q. Zhou, *Electrochim. Acta*, 2011, **56**, 7517.
32. J. Liu, C. Liu, Y. Wan, W. Liu, Z. Ma, S. Ji, J. Wang, Y. Zhou, P. Hodgson and Y. Li, *CrystEngComm*, 2013, **15**, 1578.
33. G. Zhang and X. W. Lou, *Sci. Rep.*, 2013, **3**, 1470.

34. H. Wang, Q. Gao and L. Jiang, *Small*, 2011, **7**, 2454.
35. L. Hu, L. Wu, M. Liao, X. Hu and X. Fang, *Adv. Funct. Mater.*, 2012, **22**, 998.
36. H. B. Wu, H. Pang and X. W. (David) Lou, *Energy Environ. Sci.*, 2013, **6**, 3619-3626.
37. K. Kuratani, T. kiyobayashi and N. Kuriyama, *J. Power Sources*, 2009, **189**, 1284.
38. T. Y. Wei, C. H. Chen, K. H. Chang, S. Y. Lu and C. C. Hu, *Chem. Mater.* 2009, **21**, 3228.
39. S. H. Yoon, J. W. Lee, T. Hyeon and S. M. Oh, *J. Electrochem. Soc.* 2000, **147**, 2507.
40. H. Shi, *Electrochim. Acta*, 1996, **41**, 1633.

7

ToC

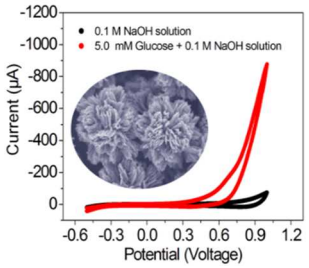

The electrode modified with mesoporous $Ni_{0.3}Co_{2.7}O_4$ hierarchical structures shows a low detection limit of 1.0 μM glucose, good sensitivity of 206.5 $mA \cdot mM^{-1} \cdot cm^{-2}$, and good selectivity.